

S&CNet: A Enhanced Coarse-to-fine Framework For Monocular Depth Completion

Lei Zhang, Weihai Chen*, Chao Hu

Abstract—Real-time depth completing is a critical problem for robotics and autonomous driving tasks. In this paper, we propose a light-weight coarse-to-fine network to complete a dense depth map from a single view RGB image and its related sparse depth map. Both the coarse estimation network and refinement network are in encoder-decoder form. To boost the performance of the coarse estimation network, we propose a novel spatial-and-channel (S&C) enhancer to boost the representation power of encoder network. The motivation for spatial-wise attention is from our finding that a lower output stride of encoder network preserve more detail but limit the receptive field. Thus, we employ spatial-wise attention to capture long-range contextual information. Besides, we found each channel in the features generated by the encoder network response to different distance. This discovery drives us to adopt channel-wise attention mechanism to reassign the weights of different channels as the decoder network should pay more attention to the channels response to distance contain rich objects, intuitively. To further improve the performance of our network, we adopt a refinement network which take the coarse estimation and sparse depth map as input. We evaluate our approach on KITTI benchmark, and the results show that our approach achieves competitive performance on RMSE metric with the state-of-the-art over published works but outperform it in all other metrics (iRMSE, MAE and iMAE) significantly with almost 3.5 times higher running speed. Crucially, our proposed S&C enhancer can be plugged into other existing models and boost their performance significantly with a minimal additional computational cost.

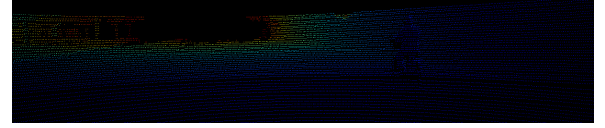
Index Terms—Attention mechaism, Dense depth completion, Coarse-to-fine framework.

I. INTRODUCTION

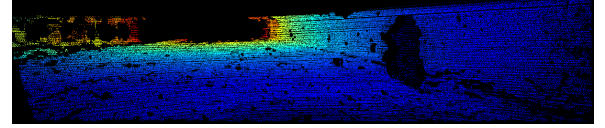
Depth sensing is essential for robotics and autonomous tasks, including obstacle avoidance and mapping. LiDAR is a popular depth sensor since it can provide high accuracy measurement even for long-range measuring. With this strength, LiDAR has been applied to a lot of robots and autonomous vehicles. However, LiDARs are still suffering from the limited number of scan lines, which makes it hard to provide dense measurements, especially for distant objects. As shown in Figure 1b, the 64-line Velodyne scan can only provide sparse depth measurement. Meanwhile, it is hard to improve the density of LiDARs measurement by increasing the scan lines as it may increase the cost sharply. Under this circumstances, estimating a dense depth map from sparse measurement has been a growing interest task. However, past research on dense depth completion has focused almost exclusively on improving accuracy, resulting in a slow inference speed. However, most



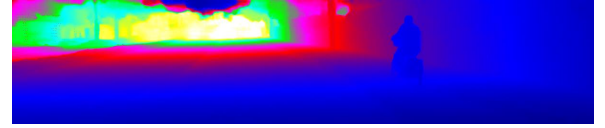
(a) raw RGB image



(b) sparse depth map



(c) semi-dense depth map



(d) generated dense depth map

Fig. 1: We develop a deep regressional network for depth completion: given (a) raw rgb color image, and (b) a sparse depth map, estimated (d) a dense depth image. Semi-dense depth labels (c) are employed as supervisor of our proposed network.

real-time systems are not only limited by computer resources but also subject to latency constraints. Therefore, a light-weight approach is essential for real-time systems. Therefore, in this paper, we focus on designing high-accuracy and light-weight network for real-time depth completion. However, a critical challenge, the trade-off between the computation complexity and inference time, keeps an algorithm from completing high accuracy dense depth map at a high running speed.

Current deep learning based state-of-the-art approaches have achieved significant improvement in accuracy [1]. However, most of them do so at the cost of increasing computational complexity [2] or by introducing other human-made supervisors [1], which result in a slow inference speed. Meanwhile, few of them has focused on designing a high accuracy algorithm with a light-weight network. Fortunately, many prior studies work on designing fast and efficient networks for image classification [3–5], segmentation [6] and object detection

Lei Zhang and Weihai Chen are with the Beihang University, Beijing, China. Emails: zhanglei2017@buaa.edu.cn, whchenbuaa@126.com Chao Hu is with the Peking University, Beijing, China. Email: 1701210857@pku.edu.cn

[7–9]. Among these works, the segmentation task is most similar to dense depth completion task as both of them can be considered as pixel-to-pixel translation problem.

Generally, sharp boundaries are essential for high-accuracy pix-to-pixel translation approaches. Recently, many works show that a lower output stride of encoder network can preserve more detail information and improve the performance of an encoder-decoder network on image segmentation task [6, 10, 11]. However, a lower output stride may limit the receptive field of the encoder network, which may result in a worse representation power, what’s worse, to accelerate the inference speed, most light-weight encoder-decoder networks employ a light-weight encoder network as the backbone. However, a light-weight encoder network is already suffering from low representation power. Once the output stride of a light-weight encoder network is decreased, the limited receptive field may further worsen the condition. Fortunately, many strategies are proposed to address this issue. [12] employed dilated convolution to increase the receptive field of convolution operation without introducing additional parameters. [13] performed pooling operations at different grid scales to extract rich semantic information. However, these improvements are not enough. To boost the performance on segmentation, [14] proposed ASPP, which can improve the performance significantly by applying several parallel atrous convolution with different rate. However, the ASPP module introduces many additional parameters and computational complexity to a framework. Recently, a non-local self-attention module, which selectively integrates the features at each position by a weighted sum of all other features at the same channel, is proposed in [15]. The working mechanism indicates that the non-local operation has a global receptive field but does not introduce too many parameters and computational complexity. Based on these insights, a non-local operation may improve the representation power of a low output stride encoder network significantly. However, the original non-local operation put much effort on reducing the computation complexity as it is usually cascaded after a heavy-weight backbone such as ResNet-101 which generate features with a huge number of channels. They do so by compressing the channels by 1×1 convolution layer, which may cause loss of information. Based on these insights, we redesign the non-local operation and adopt it as our channel-wise enhancer to boost the representation power in channel-wise.

To analysis the working mechanism of neural network based depth completing method, we study the features generated by the encoder network. Surprisingly, we notice that each channel in the generated features responds to different distance. This discovery drives us to utilize a mechanism to reassign the weights of different channels. Intuitively, not all channels should be paid the same attention in one frame. For example, if one frame contains only near objects, the channels that response to near objects should be paid more attention. Under such insight, a channel-wise attention mechanism may improve the performance of our framework. Fortunately, many channel-wise attention approaches are proposed to handle different computer vision tasks. The non-local operation can be reformed into channel-wise attention by simply transpose the

tensor of input features [10], and the reformed channel-wise attention can improve the performance on segmentation task significantly. However, many large matrix operations in this module lead to overhead computation. Squeeze-and-excitation (SE) module [16] can measure interrelationship of different channels by utilizing the channel-wise global distribution descriptor. However, this work simply adopts the popular average pooling method to generate the descriptor of global distribution, which may not robust enough to represent the global distribution of a channel. Another article [17] pointed out the same issue and adopted the variance pooling method instead. The refined SE module is utilized to handle the super-resolution task. The descriptor generated by global average pooling and global variance pooling can be considered as the representation of low-frequency signal and high-frequency signal of one channel. Although the global variance pooling method can generate a descriptor preserving high-frequency information efficiently, this approach can not handle our task, either. The reason is that the mean of one channel indicates the richness of objects in the corresponding distance, and the high-frequency signal should also be employed to preserve more detail information. Besides, by analyzing the network architecture, a convolution layer is often followed by a norm layer such as BatchNorm [18] and InstanceNorm [19]. These normalization layers assume the distribution of features like Gaussian whose distribution can be represented by a joint of mean and variance. All these insights drive us to utilize both mean and variance as the representation of global distribution but not only one of them.

Based on these insights, we present a low latency, high-throughput, high-accuracy coarse-to-fine framework for depth completion task. Specifically, we utilize a novel spatial-and-channel-wise attention based enhancer (S&C Enhancer) to boost the representation power of the light-weight encoder network. The spatial attention based enhancer is utilized to enlarge the receptive field of our encoder network. The channel attention based enhancer is employed to reassign the weight of different channels by utilizing a redesigned squeeze-and-excitation module. Moreover, we proposed a simple but efficient fusing strategy to fuse the enhancer features generated by the spatial-wise enhancer and channel-wise enhancer. Finally, we utilized a coasted hourglass module based refinement network to refine the coarse estimation generated by coarse generation network further. Our main contributions can be summarized as threefold:

- We propose a MobileNetV3 based lightweight coarse-to-fine framework to complete the dense depth map from a single RGB image and its related sparse depth map. Our algorithm achieved comparable performance on KITTI benchmark [20] with the state-of-the-art in the metrics RMSE but outperform it in all other metrics(iRMSE, iMAE, MAE and Runtime) with a 3.5 times faster running speed.
- A spatial-wise and channel-wise enhance module with few additional parameters is proposed to enhance the representation power of light-weight encoder network. Our experiment demonstrates that the proposed S&C

enhancer can be plugged into other depth completion networks easily and boost their performance significantly with minimal additional parameters.

- By studying the features, we found that the features generated by the encoder network in the depth completion task have a significant character. Each channel in the generated features responds to different distances. This discovery may be essential for explaining the working mechanism of neural network based depth completion approaches and may help other researchers generate novel strategies to boost the performance on depth completion task.

II. RELATED WORK

In this section, we summarize past research done on dense depth completion, efficient neural networks, and attention mechanism.

A. Dense Depth Completion

Completing a dense depth map from a single color image and its related sparse depth map has been an active research topic in both the robotics and computer vision communities for over a decade. Early works on depth completion task are mainly optimization based [21] or filter based methods [22]. Recently, deep learning based method has achieved significant improvement in accuracy. A fully convolution-based method is proposed to synthesize dense depth map in [23] which taking an RGB image and its related sparse depth map as input. The work [24] proposed a convolution spatial propagation network further boosted the performance on KITTI benchmark. Beyond full supervision method, [2] proposed a self-supervised training framework that requires only sequences of color and sparse depth images, without the need for dense depth labels. Recently, an impressive work [1] employed a network to estimate surface normal as the intermediate representation to produce high accuracy dense depth, and this work is the state-of-the-art approach. However, all of these methods focus heavily on attaining higher accuracy at the cost of increasing complexity and running time. Different from these works, we focusing design a framework to estimate high precision dense depth map with a light-weight architecture to make sure our algorithm can be applied in a real-time system.

B. Efficient Model Designs

From past to now, there has been a significant effort in prior works to design efficient networks. For image classification task, the *MobileNet* [3] can achieve comparable top-5 accuracy with *VGG-16* [25] on ImageNet benchmark with a 33 times fewer weights. Then, *ShuffleNet* [5] further boost the performance by adopting channel shuffle mechanism. Moreover, with the help of inverted residual structure, *MobileNetV2* [4] can outperform *MobileNet* and *ShuffleNet* with even fewer parameters. Recently, *MobileNetV3* [26] further improve the performance of efficient network by introducing the squeeze-and-excitation module. For object detection, *YOLO-V3* [9] runs 8 times faster than *Faster-RCNN* [27] and can get

higher mean average precision. For semantic segmentation task, *ERFNet* [6] employed the residual factorized convolution module, and can outperform *FCN* [28] with a 20.8 times running speed.

Among these tasks, the image segmentation task is most similar to dense depth completion task, as both of them can be considered as pixel-to-pixel translation which is mainly solved by the encoder-decoder network. However, suffering from the low representation power of the light-weight encoder network. A light-weight encoder-decoder network can hardly achieve comparable performance with heavy-weight ones. Therefore, designing a powerful feature enhancing module with few additional parameters for a light-weight encoder network is a crucial issue for a light-weight depth completion framework.

C. Attention Modules

Attention mechanisms have been widely applied in many tasks [10, 17, 29] as they can measure long-range dependencies. Specifically, [29] firstly proposed the self-attention mechanism, which can capture global dependency and contains only a few trainable parameters, for neural language processing task. Meanwhile, [15] introduced the self-attention mechanism into computer vision tasks and redesign it into non-local operation which captures spatial-wise interrelationship among all pixels in one channel. Beyond spatial-wise attention mechanisms, many works focus on measuring the correlation of features in channel-wise to boost the representation power of backbone network. For instance, squeeze-and-excitation (SE) module [16] is proposed to reassign weights of different channels by utilizing the descriptor of global distribution. However, the global descriptor used in this article is generated by simple average pooling, which may weaken the high-frequency components of images. The CAM [17] pointed out the same issue and proposed a variance pooling based SE module to improve their performance on the super-resolution task. Recently, [10] proposed channel-wise attention module which is similar to non-local operation, and jointed it with the non-local operation to boost the performance on semantic segmentation task. However, many large matrix operations in this module lead to overhead computation. In this paper, we design a new robust SE module to produce channel-wise attention and utilize the non-local operation to improve the receptive field of the encoder network. Moreover, we discuss a new approach to joint spatial-wise attention and channel-wise attention efficiently but does not introduce too much compute complexity.

III. METHODOLOGY

In this section, we describe our proposed coarse-to-fine network architecture, and the detail of our proposed S&C enhancer.

A. Network Architecture

Our proposed coarse-to-fine framework is illustrate in Figure 2. The coarse estimation network is shown in the red box, and the refinement network is shown in the green box. In the

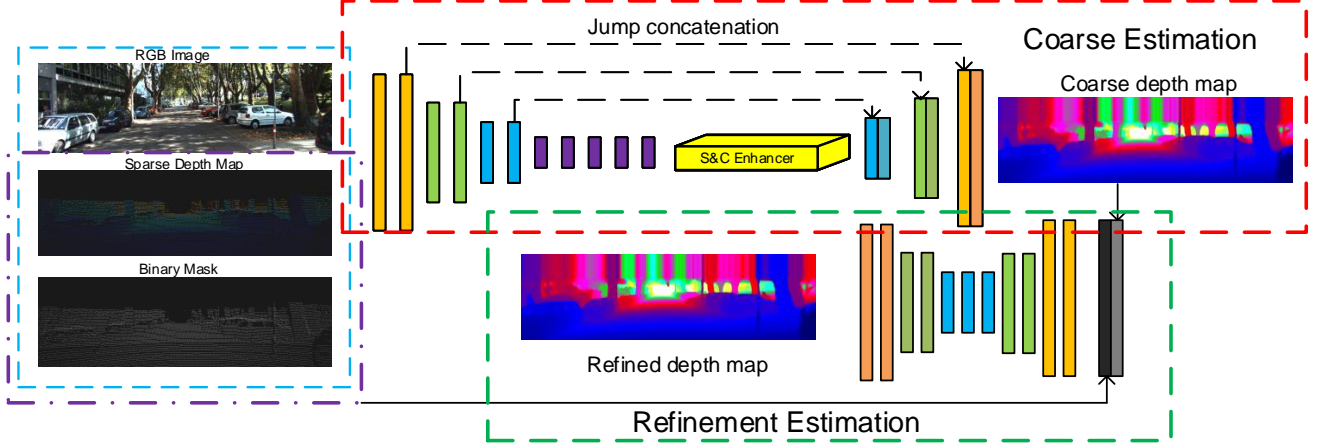


Fig. 2: Proposed network architecture. The coarse estimation network is marked with red box and the refinement network is marked with green box. The binary available map is generated from sparse depth map, if the depth of a pixel is available, the pixel in binary available map is set to 1, otherwise, it is set to 0.

coarse estimation network, a MobileNetV3-Large is employed as an encoder to extract the features from the input (raw RGB image, raw sparse depth map, and available binary mask). Where the binary available mask is generated from a sparse depth map. If the pixel's depth is available in the sparse depth map, the pixel in the binary mask is set to 1. Otherwise, it is set to 0. The output stride of the encoder is set to 8. Then, our proposed spatial and channel (S&C) enhancer, which will be illustrated in section III-B, is cascade after encoder to enhance the extracted features. Then, the enhanced features are feed into the decoder, which consists of three up-projection units as introduced in [6], to gradually increase the feature resolution. To boost the detail performance of the network, we concatenate the low-level features from encoder with the up-projected features at the same resolution. What needs to be emphasized is that we do not concatenate the low-level features from encoder directly because the corresponding low-level features usually contain a large number of channels. Instead, we apply another 1×1 convolution on the low-level features to reduce the number of channels, and then concatenate it with the corresponding decoder features.

After generated the coarse estimation, we adopt another refinement network to further improve the accuracy of the generated output. We employ two stacked hourglass network as the refinement network. Moreover, the coarse estimation output, the sparse depth map and the binary mask is concatenated as the input of the refinement network. Specifically, the RGB image is not feed into the refinement network as we expect the refinement network focus on the available pixels in the sparse depth map. With the guide of the sparse depth map, the estimated depth map can be further refined.

B. Spatial and Channel Attention Based Enhancing Module

1) *Spatial-wise enhancer*: The receptive field of our encoder network is limited since we set the output stride of the encoder to 8 to preserve more detail information. As explained in Section I, the limited receptive field can lead

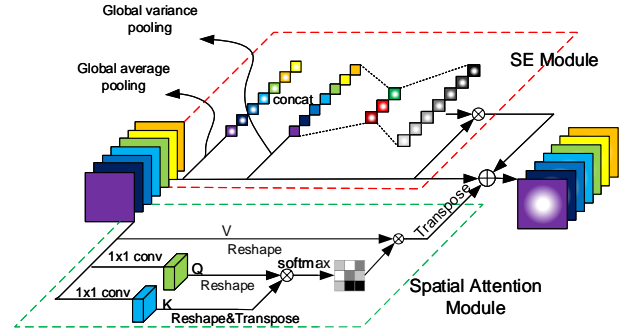


Fig. 3: Proposed S&C enhancer. The spatial-wise enhancer is marked with green box, and the channel-wise enhancer is marked with red box.

to poor performance. To address this issue, some strategies need to be carried out to enlarge the receptive field. Under such consideration, we employee the spatial-wise attention network, which is similar to non-local operation. Our spatial attention enhancer is illustrated in Figure 3 and is highlighted with the green box.

Our spatial attention mechanism can selectively integrate the features at each position by a weighted sum of all features in one channel. We denote the feature map as $A \in \mathbb{R}^{C \times H \times W}$, where C is the number of feature channels and H, W are the height and width of the feature map. At first, we feed the features map to two 1×1 convolution layers followed by BatchNorm and ReLU layers to generate the query map (Q) and key map (K). The 1×1 convolution layer reduce the number of channels by 8 times, thus Q and K is in shape of $\bar{C} \times H \times W$ where $\bar{C} = \frac{C}{8}$. The identity feature map A is employed as value map (V). Then, both the Q and K maps are reshaped to $\mathbb{R}^{\bar{C} \times N}$, where $N = H \times W$. The V is reshaped to $\mathbb{R}^{C \times N}$. Therefore, in reshaped Q and K, each pixel in the feature map can be represented by a \bar{C} dims vector. Then a

similarity between two pixels can be measured by dot product:

$$\text{similarity}(a, b) = a \cdot b \quad (1)$$

Then, the similarity map can be achieved by a matrix multiplication between the transposed \mathbf{K} and \mathbf{V} . After that, we apply a softmax layer to calculate the spatial attention map $S \in \mathbb{R}^{N \times N}$:

$$s_{ji} = \frac{\exp(K_i \cdot Q_j)}{\sum_{i=1}^N \exp(K_i \cdot Q_j)} \quad (2)$$

where s_{ji} measures the impact of the i_{th} position in value map \mathbf{V} on the j_{th} position. Note that the softmax layer indicates that more similar feature representations of the two position contribute to a greater correlation between them.

Finally, we perform a matrix multiplication between \mathbf{V} and the attention map S to generated the enhanced feature map E :

$$E_j = \sum_{i=1}^N (s_{ji} V_i) \quad (3)$$

Notice that the generated feature map E is still in the size of $\mathbb{R}^{C \times N}$. Thus it should be reshaped into the size of $\mathbb{R}^{C \times H \times W}$ to generate the spatial enhanced feature map.

It can be inferred from Equation 3 that the enhanced feature \mathbf{E} at each position is a weighted sum of the all features in one channel. Therefore, the spatial enhancer has a global contextual view. Thus it can enlarge the receptive field. Besides, similar represented features achieve mutual gains.

Note that there is some difference between our spatial attention module and non-local operations. Since the non-local operation in [15] is added after a heavy-weight backbone, the features need to be enhanced contain a large number (1024) of channels. To reduce the memory cost, they first compress the number of the channel to half (512) by 1×1 convolution layer to generate the query map (\mathbf{Q}), key map (\mathbf{K}) and value map (\mathbf{V}). At the end of the non-local module, another 1×1 convolution layer is applied to project the number of channels back to 1024. However, the compress-and-project operation may cause a loss of information. As we employed a MobileNet-V3 network as a backbone, there exist only 160 channels in the generated feature map. Therefore, the compress-and-project operation is not quite necessary for our approach. However, we still applied two 1×1 convolution layer to generate query map (\mathbf{Q}), key map (\mathbf{K}) with fewer channels as [30] point out a reducing channel number on map \mathbf{Q} and \mathbf{K} will not worsen the performance significantly. Based on these insights, we reduce the channel number of \mathbf{Q} and \mathbf{K} to $\frac{C}{8}$ for memory efficiency but employee identity feature map \mathbf{A} as \mathbf{V} directly to preserve more information.

2) *Channel-wise enhancer.*: In section III-B1, we introduce the spatial-wise attention mechanism to enlarge the receptive field of our backbone. Meanwhile, the representation power can be further boosted by a channel-wise enhancer. By studying the features generated by the encoder network in our approach, we find that each channel in the feature maps has a different response amplitude to different distance objects. Some example is shown is Figure 4. Based on this discovery, we propose that not all of the channels should be paid the same attention. For example, if one frame mainly contains close

objects, the decoder should pay more attention to the channels which response more actively to close objects. On the contrary, if one frame mainly contains far objects, the decoder should pay more attention to the channels response to far distance. This discovery drives us to adopt some strategies to measure the channel-wise relationship of generated features.

Based on these insights, a channel-wise attention mechanism should improve the performance on depth completion task significantly. Meanwhile, several recent approaches have shown the benefit of modeling the channel relationship in computer vision tasks. However, some approaches of them will introduce too much additional computation into a network. As we are aiming at designing a fast and light-weight network, efficiency is the most important factor in our consideration. Among the approaches in channel-wise attention mechanism, the squeeze-and-excitation networks is an efficient and low-latency method. This approach measures the channel relationship by first squeeze the features in channel-wise to get a descriptor of the global distribution of each channel, and then generate the weights of channels by two cascaded fully connected layer. However, this work simply adopts the popular average pooling method to generate the descriptor of global distribution, which may not robust enough to represent the global distribution of a channel. Another article [17] pointed out the same issue and adopted the variance pooling method instead of super-resolution task. However, we argue that both of these methods may be not robust enough for our task. As shown in Figure 5, we have shown some toy example to illustrate our argument. Intuitively, descriptor generated by global average pooling while global variance pooling can be considered as the representation of low-frequency signal and high-frequency signal of one channel. That's maybe the reason why mean descriptor works well for classification task and variance descriptor works well for super-resolution task. However, in our task, the mean and variance information are both important. As mentioned before, each channel in the feature maps has a different response amplitude to different distance. Therefore, the mean of one channel can be considered as a descriptor of the richness of objects in the corresponding distance range. And the variance of one channel can preserve more detail information which can help the decoder generator more clear boundaries. Moreover, the nowadays network often add a norm layer (BatchNorm, InstanceNorm, etc.) after every convolution layer. Take the BatchNorm as an example, its operation can be written as:

$$\hat{y}_i = \gamma \frac{x_i - \mu_\beta}{\sqrt{\sigma_\beta^2 + \epsilon}} + \beta \quad (4)$$

in which, the distribution of layers is assumed to be Gaussian distribution which can be represented by variance and mean, and is normalized by the scale variance γ and shift mean β . Therefore, a combination of variance and mean of one channel is a robust way to represent the distribution. These insights drive us to fuse global mean and global variance of a layer as the descriptor of the global distribution. Then the redesigned SE module is shown as fellow:

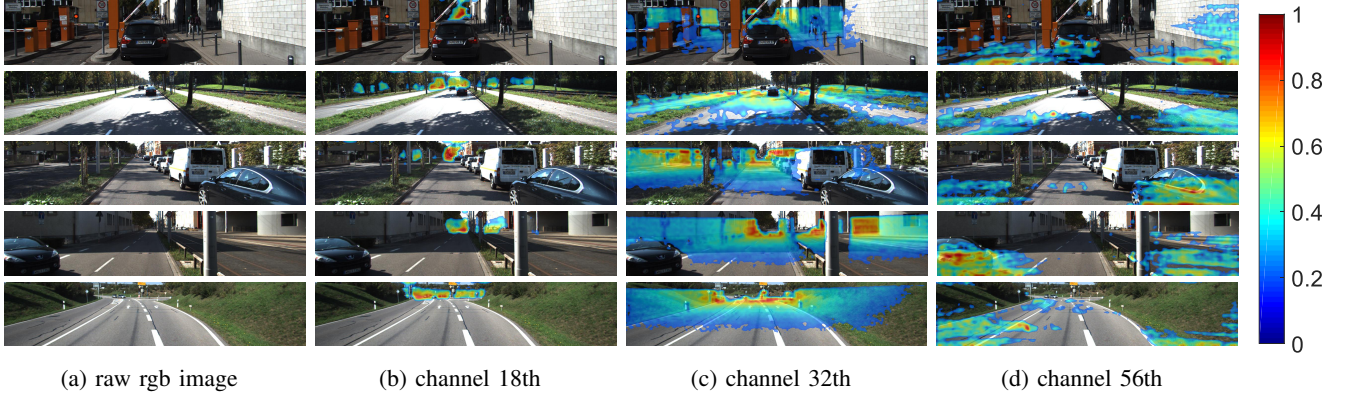


Fig. 4: Visualization of the intermediate feature map. As shown in the figure above, the 18th channel of our feature map response to long-distance objects, the 32th feature map response to middle distance objects and the 56th response to near objects.

Squeeze. Now we assume that the features need to be enhanced as $\mathbf{A} \in \mathbb{R}^{C \times H \times W}$. To measure the channel interrelationship, we first consider each channel in the feature map. We follow the setting of [16] to squeeze global spatial information into a channel descriptor. Different from [16], we generate the channel descriptor by utilizing both of the global average pooling and global variance pooling. The channel-wise statistics are generated by concatenating the mean and variance of a channel. The statistic of channel can be written as $\mathbf{z} = [\mathbf{z}_c^{\text{mean}} \ \mathbf{z}_c^{\text{var}}] \in \mathbb{R}^{2C}$. Where $\mathbf{z}_c^{\text{mean}} \in \mathbb{R}^C$ and $\mathbf{z}_c^{\text{var}} \in \mathbb{R}^C$ are the channel-wise mean and variance descriptor. And the statistic is archived by shrinking \mathbf{A} through its spatial dimensions $H \times W$. Then, the c -th element of \mathbf{z} is calculated by:

$$z_c^{\text{mean}} = F_{sq}(\mathbf{a}_c) = \frac{1}{H \times W} \sum_{i=1}^H \sum_{j=1}^H a_c(i, j) \quad (5)$$

$$z_c^{\text{var}} = F_{sq}(\mathbf{a}_c) = \frac{1}{H \times W} \sum_{i=1}^H \sum_{j=1}^H (a_c(i, j) - z_c^{\text{mean}})^2 \quad (6)$$

where \mathbf{a}_c the c -th channel in the features \mathbf{A} and $a_c(i, j)$ is the feature at position (i, j) in \mathbf{a}_c .

Excitation. After generated the global channel-wise descriptor. The excitation and scaling processes are performed in the [16]. The excitation employee simple gating mechanism with a sigmoid activation to generate the weights of channels:

$$\mathbf{s} = \mathbf{F}(\mathbf{z}, \mathbf{W}) = \sigma(g(\mathbf{z}, \mathbf{W})) = \sigma(\mathbf{W}_2 \delta(\mathbf{W}_1 \mathbf{z})) \quad (7)$$

where $\mathbf{s} \in \mathbb{R}^C$ is the generated weight of features \mathbf{A} . $\mathbf{W}_1 \in \mathbb{R}^{\frac{2C}{r} \times 2C}$ and $\mathbf{W}_2 \in \mathbb{R}^{C \times \frac{2C}{r}}$ are the parameters of two non-biased fully-connected layers. δ and σ refers to the ReLU and Sigmoid activation layer. And \mathbf{z} is concatenated by the global mean statics \mathbf{z}^{mean} and the global variance statics \mathbf{z}^{var} . The first FC layer reduce the dimension from $2C$ to $\frac{2C}{r}$ with reduction ratio r . A ReLU activation layer is added after the first FC layer and the followed by another FC layer expend the dimension back to the number of channels C . Then, the output of second FC layer is activated by a *Sigmoid* activation layer to limit the out to the range of $[0, 1]$. Finally, the channel wise

enhanced features $\mathbf{X} \in \mathbb{R}^{C \times H \times W}$ is obtained by resealing \mathbf{A} with the weights \mathbf{s} :

$$\mathbf{x}_c = F(\mathbf{a}_c, s_c) = s_c \mathbf{u}_c \quad (8)$$

where \mathbf{x}_c is the c -th channel in the channel-wise enhanced feature \mathbf{A} .

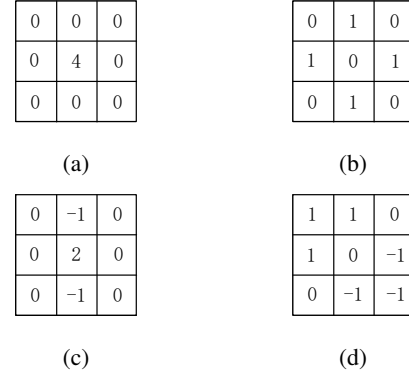


Fig. 5: (a) and (b) share the same mean by their global distributions are entirely different. (c) and (d) share the same variance, but their global distributions are different neither.

C. Fusing

The proposed channel-wise enhancer and spatial-wise enhancer utilize information from inter-channel and intra-channel relationship. However, the strategy to fuse the enhanced feature map is also a critical problem. Directly concatenate the two enhanced feature maps can exploit the benefits of both mechanisms mostly. However, this strategy will introduce too many additional parameters which may slow down the inference speed of the entire network. To make use of both mechanisms simultaneously, we further multiply the two enhanced features by trainable scale parameters and add back the identity feature map. Therefore, the final enhanced feature map is given by:

$$\mathbf{Y} = \lambda \mathbf{E} + \gamma \mathbf{X} + \mathbf{A} \quad (9)$$

where the \mathbf{Y} is the final output of S&C enhancer, \mathbf{E} is the output of the spatial wise attention module, \mathbf{X} is the output of

channel wise attention module and the \mathbf{A} is the identity feature map. Beyond the proposed fusing strategy, we also tried other strategies to fuse the features, and the compare experiment is shown in Section IV-D.

IV. EXPERIMENTS

In this section, we present the experimental result to demonstrate our approach and the boosting power of our proposed S&C enhancer. We first present an evaluation against existing published work on KITTI on-line benchmark. Then we provide an ablation study of our design to analyze the influence of each component. Moreover, to demonstrate the boosting power of our proposed S&C enhancer, we plug this module into the existing network and compare the evaluation result against the original network.

A. Datasets and Metrics

We train our networks and evaluate their accuracy on the KITTI dense depth completion dataset [20] with the official train/validation data split. The datasets are collected using two HD camera and Velodyne 64-line LiDARs. This dataset includes semi-dense annotations, RGB image, and sparse depth map. In detail, it contains 86k images for training, 3k images for testing and 4k images for validation. Moreover, all splits are ensured a similar distribution over KITTI scene categories. To evaluate the performance, we utilize the metrics provided by KITTI on-line benchmark. They are:

- **iRMSE**: Root mean squared error of the inverse depth $[1/km]$
- **iMAE**: Mean absolute error if the inverse depth $[1/km]$
- **RMSE**: Root mean squared error $[mm]$
- **MAE**: Mean absolute error $[mm]$
- **Runtime**: Time cost for inference one frame $[s]$

B. Implementation Details

We implement our model using *PyTorch* [31]. Our framework contains two sub-networks: the coarse estimation network and the refinement network. Both of the two networks are in encoder-decoder form. In coarse generation network, we adopt a MobileNetV3-Large [26] implementation as our backbone encoder network. What needs to be emphasized is that we set the output stride of MobileNetV3-Large to 8 instead of 32. We achieve this by setting the output stride of the 2nd and 13th "bneck" module to 1 instead of 2 in original. The backbone network is pre-trained on the ImageNet dataset [32]. Then, we adopt the proposed S&C enhancer after the encoder network to enhance the features. After this, we utilize the up projection module proposed in [6] to generate the coarse estimation depth map. In the end, we adopt two cascaded stacked hourglass network [33] as the refinement network.

The network is trained with 32-bit floating point precision. For training, a batch size of 16 and a learning rate of 0.001 are used. Adam [34] is employed as optimizer. Furthermore, we crop the inputs to a resolution of 256×1216 since the LiDAR frame does not provide any information at the top. And the

MSE (mean squared error) is employed as the loss function of our model. Then, the loss function is given by:

$$\begin{aligned} Loss_{depth}(pred_{coarse}, pred_{refine}, d) \\ = \alpha ||\mathbb{I}_{d>0} \cdot (pred_{coarse} - d)||_2^2 \\ + \beta ||\mathbb{I}_{d>0} \cdot (pred_{refine} - d)||_2^2 \end{aligned} \quad (10)$$

where $pred_{coarse}$ is the dense depth map generated by the coarse estimation network and $pred_{refine}$ is the refined depth map. Note that we only calculate the pixels whose depth information is provided in the groundtruth dense depth map. The α and β are weights of coarse result and refined result which is set to be 0.3 and 0.7.

C. Comparison with Previous Methods

In this section, we train our best network for KITTI benchmark against other published results. We use the official error metrics for the KITTI depth completion benchmark, including *rmse*, *mae*, *irmse*, and *imae*. Specifically, *rmse* and *mae* stand for the root-mean-square error and the mean absolute error, *irmse* and *imae* stand for the root-mean-square error and the mean absolute error in the inverse depth representation. The result are listed in Table II and visualized in Figure 6.

As shown in Table II, our approach ranking the second over the published works on KITTI benchmark. Moreover, our approach achieve comparable performance with the published state-of-the-art in the ranking metric *RMSE* but outperform than it in all other metrics with a much higher inference speed. DDP [37] performs best in metrics *iRMSE*, *iMAE* and *MAE* as they employed *MAE* since their loss function. However, their performance on the main metric *RMSE* is much worse than state-of-the-art. The fast approaches [35, 36] run much faster than state-of-the-art, but their performance on metrics are much worse. Note that [38] achieved a good balance between accuracy and speed. However, our approach outperforms it in all metrics with a similar running speed.

Moreover, our estimated depth image also have a cleaner and sharper object boundaries even compare with the state-of-the-art, which can be attributed to the fact that our S&C model boosts the representation power of our encoder network and the lower output stride of backbone network can preserve more image details. For example, see the car's window in left-bottom of the first picture and the car's window in right-bottom of the third picture. Note that we trained our network with an input size of 1216×256 because the 30% semi-dense annotations do not contain labels in these top regions. At the evaluation, we just expand the image into the resolution of 1216×352 by copy the top row of the original output depth map.

D. Ablation Studies

To analyze the influence of network components on performance, we conduct a detailed ablation by testing each component in the framework and their combinations to see how they contribute to the estimation precision. The ablation study is done one the KITTI selected cropped validation dataset. The detailed results under different experimental conditions

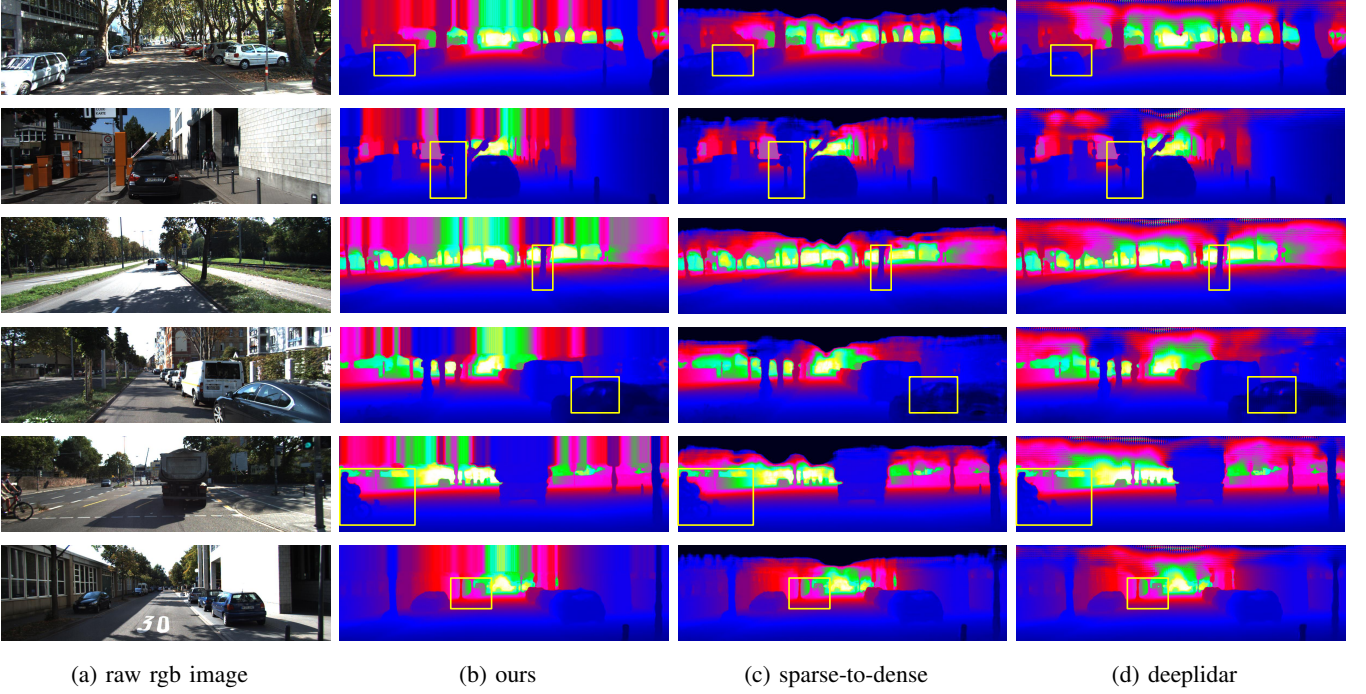


Fig. 6: Visual comparison with state-of-the-art. The yellow box shows the area to focus on in the depth map. Our approach shows sharper boundaries. For example, see the car’s window in the first and third row

TABLE I: Ablation study of the framework for dense depth completion. The sign \checkmark indicate that this module is added into the framework. Besides, the best and the second best records are marked as **bold** and **blue**.

output stride (OS)	skip connection	spatial attention	channel attention	fusing	refinement network	RMSE
$OS = 8$	\checkmark	\checkmark	proposed	proposed	\checkmark	786.32
$OS = 8$	\checkmark	\checkmark	mean	proposed	\checkmark	793.82
$OS = 8$	\checkmark	\checkmark	variance	proposed	\checkmark	794s.40
$OS = 8$	\checkmark	\checkmark	proposed	concat	\checkmark	785.25
$OS = 8$		\checkmark	proposed	proposed	\checkmark	796.13
$OS = 8$			proposed	proposed	\checkmark	815.32
$OS = 8$					\checkmark	831.02
$OS = 8$						879.33
$OS = 16$	\checkmark	\checkmark	proposed	proposed	\checkmark	794.80
$OS = 16$	\checkmark	\checkmark	mean	proposed	\checkmark	801.08
$OS = 16$	\checkmark	\checkmark	variance	proposed	\checkmark	804.79
$OS = 16$	\checkmark	\checkmark	proposed	concat	\checkmark	795.21
$OS = 16$		\checkmark	proposed	proposed	\checkmark	817.02
$OS = 16$			proposed	proposed	\checkmark	821.32
$OS = 16$					\checkmark	848.32
$OS = 16$						884.77

TABLE II: Comparisons to the state-of-the-art dense depth completion on the on-line KITTI benchmark. For all metrics, lower is better. The best and the second best records are marked as **bold** and **blue**.

on KITTI benchmark	iRMSE	iMAE	RMSE	MAE	Runtime[ms]
CSPN <i>et al.</i> [24]	2.93	1.15	1019.64	279.46	1000
DFineNet <i>et al.</i> [35]	3.21	1.39	943.89	304.17	20
NConv-CNN-L1 <i>et al.</i> [36]	2.52	0.92	859.22	207.77	20
NConv-CNN-L2 <i>et al.</i> [36]	2.60	1.03	829.98	233.26	20
DDP <i>et al.</i> [37]	2.10	0.85	832.94	203.96	80
Sparse-to-Dense (gd) <i>et al.</i> [2]	2.80	1.21	814.73	249.95	80
RGB guidececertainty <i>et al.</i> [38]	2.19	0.93	772.87	215.02	20
DeepLidar <i>et al.</i> [1]	2.56	1.15	758.38	226.50	70
This Work	2.12	0.90	759.64	210.33	20

are listed in Table I. The experiment condition is listed in the first row of Table I. The illustration of the experiment condition is listed below:

- **output stride**: this column stands for the output stride of

encoder network in coarse estimation network. $OS = 8$ indicate we set the output stride of MobileNetV3-Large by setting the output stride of both *2nd* and *13th* *bneck* operator to 1 instead of 2 in original. $OS = 16$ indicate we set the output stride of MobileNetV3-Large by setting only the *13th* *bneck* operator to 1.

- **skip connection**: the \checkmark stand for we add skip connection between encoder and decoder in the coarse generation module. On the contrary, Blank indicates the skip connection is not employed.
- **spatial attention** \checkmark stands for we plugged the proposed channel attention at the end of MobileNetV3-Large, and blank indicates the spatial attention enhancer is not adopted.
- **channel attention**: *proposed* indicate we plugged the proposed channel-wise attention module into the coarse generation network. *mean* indicate the SE module pro-

posed in [16] is adopted. *variance* indicate the SE module proposed in [17] is employed. Blank indicates there is no channel attention module in our network.

- **fusing proposed** indicate we adopt the proposed strategy to fuse the enhanced features generated by channel and spatial enhancer. *concat* indicate we simply concatenate the spatial and channel enhanced features.
- **refinement network** this column shows we adopt the refinement network or not. \checkmark indicate the refinement network is adopted and blank indicate not.

By analyzing Table I, we can conclude that the most effective components in improving final accuracy include using proposed S&C enhancer and adding the cascade refinement network. Besides, adding skip connections between the encoder and decoder networks in coarse estimation network, decrease the output stride of backbone also in substantial improvement. Meanwhile, we test different strategies to fuse the enhanced feature map generated by the spatial enhancer and channel enhancer. The experiment result shows that the concatenation strategy only improved the result a bit little than our proposed fusing strategy but it will introduce much more parameters and a lot of computational complexity. Besides, our proposed channel-wise attention mechanism do dose better in our task than the SE module proposed in [17] and [16], the result can be inferred in line 1st, 2th, 3th in the block **OS = 8** and block **OS = 16**. What is interested is that at the condition **OS = 8**, the mean based SE module and variance based module performs quite similar. However, when **OS = 8**, the mean based SE module performs much better than the variance based module. This phenomenon may be caused by the loss of detail information when **OS** goes high. Besides, by analyzing the first block and second block in Table I, we can conclude that a lower **OS** can also improve the performance in our task

Furthermore, we also tested the additional regularization, such as weight decay, leads to degraded performance. However, adding dropout do improve the performance on validation and testing dataset. Moreover, it is worth noting that alternative decoding method of the enhanced feature map (such as nearest neighbor interpolation or the bilinear interpolation) does not improve the estimation accuracy.

E. Analysis of Spatial Attention Module

We utilized redesigned non-local operation as our spatial attention enhancer to enlarge the receptive field of our encoder network. To analyze the influence of our spatial enhancer. We visualize the attention maps produced by spatial enhancer, which are shown in Figure 7. The first column is the raw RGB image. The second and third column is the visualized attention of spatial enhancer. The corresponding point of the visualized attention map is marked with red dots. It can be found that the spatial enhancer can integrate features in a global view with their relationship regardless of their distance.

F. Analysis of Channel Attention Module

The channel attention mechanism is adapted to reset the weight of channels. As mentioned previous, each channel

response to different distance. To analyze the influence of our channel enhancer module. We visualized the channels responding to different distance, and we visualized the weight of them, which are shown in Figure. 9. The first column is the raw RGB image. The second column is the 18th channel which response to far objects. The third column is the 18th channel in feature map which response to middle-distance objects and the fourth column is the 56th channel response to near objects. The activation map is visualized in the jet color map and applied on the RGB image. The weights generated by channel enhancer is written in the caption under the picture. It can be found that the channel enhancer can reassign the weight of channels from an attention-based mechanism. As shown in the first row of Figure. 9. This frame contains only a few far objects, thus the weight of the 18th channel is significantly lower than the frame shown in the second and third row. Besides, this frame contains a lot of near objects, thus the weight of the 56th channel is higher than the others. All of the pictures mainly contain objects in the middle distance, therefore, the 32th channel is paid the highest attention.

TABLE III: The compare result of original model, finetuned model and finetuned model after adding the proposed S&C enhancer.

(a) The compare result of work sparse-to-dense [2]

Model	RMSE	Parameters (Million)	Inference time
Original	858	26.107	78.6
Finetuned	855	26.107	78.6
Enhanced	806	26.485	79.9

(b) The compare result of work RGB-guideconfidence [38]

Model	RMSE	Parameters (Million)	Inference time (ms)
Original	802	2.545	19.8
Fineuned	804	2.545	19.8
Enhanced	791	2.568	20.4

TABLE IV: Comparisons of sparse-to-dense and enhanced sparse-to-dense on the KITTI benchmark.

on KITTI benchmark	iRMSE	iMAE	RMSE	MAE	Runtime[ms]
Original	2.60	1.21	814.73	249.95	80
Enhanced	2.40	1.08	772.66	231.89	80

G. Further Analysis of the S&C Enhancer

The previous experiment result has demonstrated the improvement of our proposed S&C enhancer in our network. Meanwhile, our proposed S&C enhancer can be easily plugged into existing deep architectures and produce significant performance improvements but introduce only a minimal additional computational cost. To demonstrate the boosting power of our proposed S&C enhancer, we investigate the effect of plugging S&C enhancer into another two existing architectures, sparse-to-dense [2] and confidence-guidance [38]. We first download the pre-trained model of these two networks and implement two ablation studies over these two networks. We fine-tuned the two pre-trained models directly for ten epochs with the default training strategy at first. Then, as a comparison, we plug the proposed S&C enhancer at the end of the encoder in the two architectures and fine-tuned the enhanced models for ten epochs from the download parameters. We evaluate

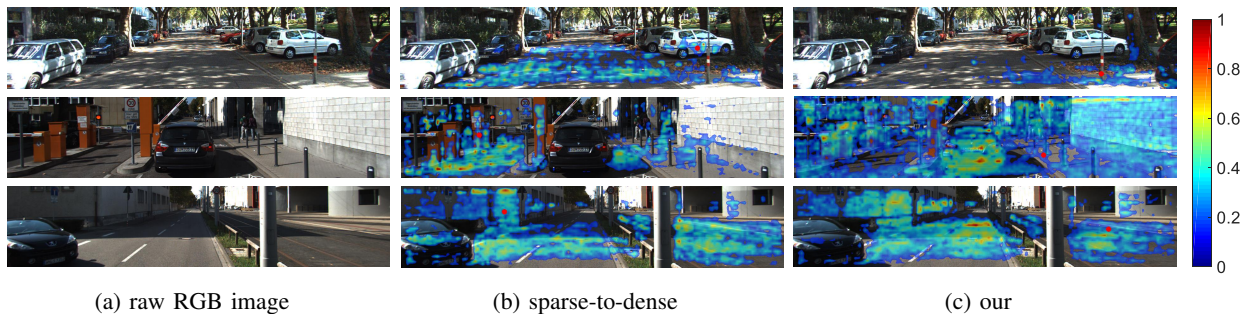


Fig. 7: The attention map is visualized by jet colormap and the generated colormap is applied on the RGB image. The corresponding points of visualized attention map are marked with red dots.

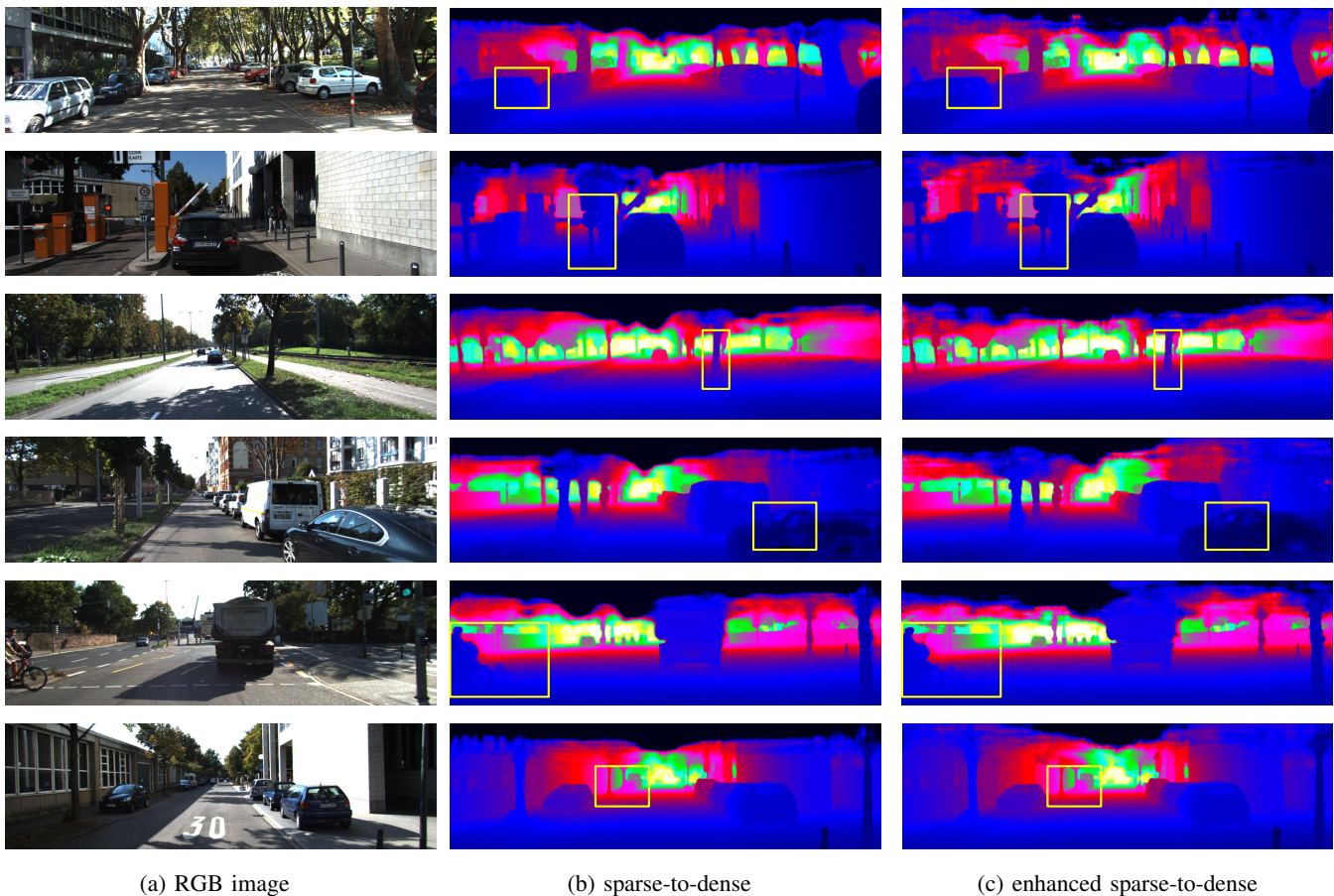


Fig. 8: Comparison against original sparse-to-dense. The enhanced approach perform not only higher accuracy, but also cleaner boundaries.

the results of both networks in the KITTI selected cropped validation dataset. Meanwhile, we submit the testing result of enhancer sparse-to-dense [2] to the KITTI on-line benchmark.

The finetuned result in KITTI selected cropped validation dataset is listed in Table III. In the column **Model**, *Original* indicates the performance of the downloaded model, *Finetuned* stands for the fine-tuned model without proposed S&C enhancer and "Enhanced" stand for the fine-tuned model after plugged the proposed S&C enhancer. For sparse-to-dense, the proposed S&C enhancer improved the RMSE from $858mm$ to $806mm$ with only 0.378 million additional parameters. For RGB-guideconfidence, the proposed S&C enhancer improved the RMSE from $802mm$ to $791mm$ with only 0.023 million

additional parameters.

Besides, we submit the result of enhanced sparse-to-dense on KITTI on-line benchmark and the performance is improved significantly. The compare result of metrics is listed in Table IV and the compare result is shown in Figure 6b. For sparse-to-dense, our S&C enhancer improves RMSE from $814.73mm$ to $772.66mm$. With the plugged S&C enhancer, the ranking of sparse-to-dense it improved from 19th to 9th.

V. CONCLUSION

We propose a coarse-to-fine network to estimate high accuracy dense depth map from a single view RGB image and

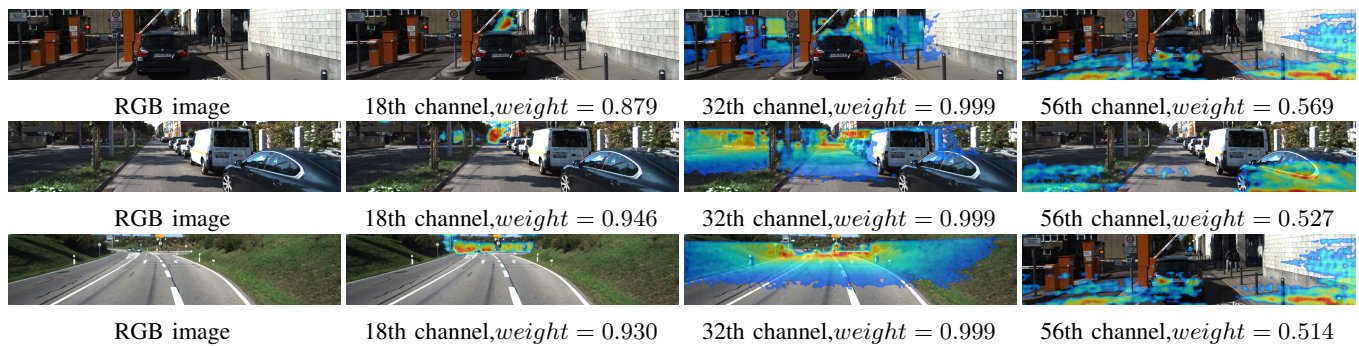


Fig. 9: The features activation map is converted from gray to the jet color map, and the converted color map is applied on RGB image. The first column is RGB images. The 2nd,3rd,4th columns are the visualization of 18th,32th,56th channels in feature map generated by MobileNetV3-Large. The 18th, 32th and 56th channel response to far objects, mid-distance objects and near objects. The weights of each channel generated by channel enhancer is shown in the caption of each picture.

its related sparse depth map. For real-time requirements for self-driving cars with a large margin, we choose a lightweight network MobileNetV3-Large as the backbone which suffers from the lower representation power than heavier ones like ResNet. To boost the representation power of the backbone, we proposed S&C enhancer. Moreover, a casted hourglass network is employed as a refinement network to refine the output depth map of our coarse estimation network. With all these techniques, our model finally achieves competitive accuracy performance with the state-of-the-art on $RMSE$ metric but outperform it in all other metrics ($iRMSE, iMAE, MAE$) significantly with almost 3.5 times running speed. Moreover, our experiment demonstrates that our proposed S&C enhancer can be easily plugged into other existing networks and boost their performance on the depth completion task significantly with a minimal additional parameter.

REFERENCES

- [1] J. Qiu, Z. Cui, Y. Zhang, X. Zhang, S. Liu, B. Zeng, and M. Pollefeys, “Deeplidar: Deep surface normal guided depth prediction for outdoor scene from sparse lidar data and single color image,” *arXiv: Computer Vision and Pattern Recognition*, 2018.
- [2] F. Ma, G. V. Cavalheiro, and S. Karaman, “Self-supervised sparse-to-dense: Self-supervised depth completion from lidar and monocular camera,” *arXiv: Computer Vision and Pattern Recognition*, 2018.
- [3] A. Howard, M. Zhu, B. Chen, D. Kalenichenko, W. Wang, T. Weyand, M. Andreetto, and H. Adam, “Mobilenets: Efficient convolutional neural networks for mobile vision applications,” *arXiv: Computer Vision and Pattern Recognition*, 2017.
- [4] M. Sandler, A. Howard, M. Zhu, A. Zhmoginov, and L. Chen, “Mobilenetv2: Inverted residuals and linear bottlenecks,” *computer vision and pattern recognition*, pp. 4510–4520, 2018.
- [5] M. G. Hluchyj and M. J. Karol, “Shuffle net: an application of generalized perfect shuffles to multihop lightwave networks,” *Journal of Lightwave Technology*, vol. 9, no. 10, pp. 1386–1397, 1991.
- [6] E. Romera, J. M. Alvarez, L. M. Bergasa, and R. Arroyo, “Erfnet: Efficient residual factorized convnet for real-time semantic segmentation,” *IEEE Transactions on Intelligent Transportation Systems*, vol. 19, no. 1, pp. 263–272, 2018.
- [7] W. Liu, D. Anguelov, D. Erhan, C. Szegedy, S. E. Reed, C. Fu, and A. C. Berg, “Ssd: Single shot multibox detector,” *European conference on computer vision*, pp. 21–37, 2016.
- [8] J. Redmon, S. K. Divvala, R. B. Girshick, and A. Farhadi, “You only look once: Unified, real-time object detection.”
- [9] J. Redmon and A. Farhadi, “Yolov3: An incremental improvement,” *arXiv: Computer Vision and Pattern Recognition*, 2018.
- [10] J. Fu, J. Liu, H. Tian, Z. Fang, and H. Lu, “Dual attention network for scene segmentation,” *arXiv: Computer Vision and Pattern Recognition*, 2018.
- [11] L.-C. Chen, Y. Zhu, G. Papandreou, F. Schroff, and H. Adam, “Encoder-decoder with atrous separable convolution for semantic image segmentation,” pp. 801–818, 2018.
- [12] F. Yu and V. Koltun, “Multi-scale context aggregation by dilated convolutions,” *international conference on learning representations*, 2016.
- [13] H. Zhao, J. Shi, X. Qi, X. Wang, and J. Jia, “Pyramid scene parsing network,” *computer vision and pattern recognition*, pp. 6230–6239, 2017.
- [14] L. Chen, G. Papandreou, F. Schroff, and H. Adam, “Rethinking atrous convolution for semantic image segmentation,” *arXiv: Computer Vision and Pattern Recognition*, 2017.
- [15] X. Wang, R. B. Girshick, A. Gupta, and K. He, “Non-local neural networks,” *computer vision and pattern recognition*, pp. 7794–7803, 2018.
- [16] J. Hu, L. Shen, and G. Sun, “Squeeze-and-excitation networks,” *computer vision and pattern recognition*, pp. 7132–7141, 2018.
- [17] J. Kim, J. Choi, M. Cheon, and J. Lee, “Ram: Residual attention module for single image super-resolution,” *arXiv: Computer Vision and Pattern Recognition*, 2018.
- [18] S. Ioffe and C. Szegedy, “Batch normalization: Accelerat-

- ing deep network training by reducing internal covariate shift,” *international conference on machine learning*, pp. 448–456, 2015.
- [19] D. Ulyanov, A. Vedaldi, and V. S. Lempitsky, “Instance normalization: The missing ingredient for fast stylization,” *arXiv: Computer Vision and Pattern Recognition*, 2016.
- [20] A. Geiger, P. Lenz, C. Stiller, and R. Urtasun, “Vision meets robotics: The kitti dataset,” *The International Journal of Robotics Research*, vol. 32, no. 11, pp. 1231–1237, 2013.
- [21] J. Park, H. Kim, Y. Tai, M. S. Brown, and I. S. Kweon, “High-quality depth map upsampling and completion for rgb-d cameras,” *IEEE Transactions on Image Processing*, vol. 23, no. 12, pp. 5559–5572, 2014.
- [22] C. Richardt, C. Stoll, N. A. Dodgson, H. Seidel, and C. Theobalt, “Coherent spatiotemporal filtering, upsampling and rendering of rgbz videos,” *Computer Graphics Forum*, vol. 31, no. 2, pp. 247–256, 2012.
- [23] J. Uhrig, N. Schneider, L. Schneider, U. Franke, T. Brox, and A. Geiger, “Sparsity invariant cnns,” *international conference on 3d vision*, pp. 11–20, 2017.
- [24] X. Cheng, P. Wang, and R. Yang, “Depth estimation via affinity learned with convolutional spatial propagation network,” *european conference on computer vision*, pp. 108–125, 2018.
- [25] K. Simonyan and A. Zisserman, “Very deep convolutional networks for large-scale image recognition,” *international conference on learning representations*, 2015.
- [26] A. Howard, M. B. Sandler, G. Chu, L. Chen, B. Chen, M. Tan, W. Wang, Y. Zhu, R. Pang, V. Vasudevan *et al.*, “Searching for mobilenetv3,” *arXiv: Computer Vision and Pattern Recognition*, 2019.
- [27] S. Ren, K. He, R. B. Girshick, and J. Sun, “Faster r-cnn: Towards real-time object detection with region proposal networks,” *IEEE Transactions on Pattern Analysis and Machine Intelligence*, vol. 39, no. 6, pp. 1137–1149, 2017.
- [28] J. Long, E. Shelhamer, and T. Darrell, “Fully convolutional networks for semantic segmentation,” pp. 3431–3440, 2015.
- [29] A. Vaswani, N. Shazeer, N. Parmar, J. Uszkoreit, L. Jones, A. N. Gomez, Ł. Kaiser, and I. Polosukhin, “Attention is all you need,” pp. 5998–6008, 2017.
- [30] H. Zhang, I. Goodfellow, D. Metaxas, and A. Odena, “Self-attention generative adversarial networks,” *arXiv preprint arXiv:1805.08318*, 2018.
- [31] A. Paszke, S. Gross, S. Chintala, and G. Chanan, “Pytorch: Tensors and dynamic neural networks in python with strong gpu acceleration,” *PyTorch: Tensors and dynamic neural networks in Python with strong GPU acceleration*, vol. 6, 2017.
- [32] J. Deng, W. Dong, R. Socher, L.-J. Li, K. Li, and L. Fei-Fei, “Imagenet: A large-scale hierarchical image database,” pp. 248–255, 2009.
- [33] A. Newell, K. Yang, and J. Deng, “Stacked hourglass networks for human pose estimation,” pp. 483–499, 2016.
- [34] D. P. Kingma and J. Ba, “Adam: A method for stochastic optimization,” *arXiv preprint arXiv:1412.6980*, 2014.
- [35] Y. Zhang, T. Nguyen, I. D. Miller, S. Chen, C. J. Taylor, V. Kumar *et al.*, “Dfinenet: Ego-motion estimation and depth refinement from sparse, noisy depth input with rgb guidance,” *arXiv preprint arXiv:1903.06397*, 2019.
- [36] A. Eldesokey, M. Felsberg, and F. S. Khan, “Confidence propagation through cnns for guided sparse depth regression,” *arXiv preprint arXiv:1811.01791*, 2018.
- [37] Y. Yang, A. Wong, and S. Soatto, “Dense depth posterior (ddp) from single image and sparse range,” *arXiv: Computer Vision and Pattern Recognition*, 2019.
- [38] W. Van Gansbeke, D. Neven, B. De Brabandere, and L. Van Gool, “Sparse and noisy lidar completion with rgb guidance and uncertainty,” *arXiv preprint arXiv:1902.05356*, 2019.
- [39] X. Zhang, X. Zhou, M. Lin, and J. Sun, “Shufflenet: An extremely efficient convolutional neural network for mobile devices,” *computer vision and pattern recognition*, pp. 6848–6856, 2018.
- [40] M. Jaritz, R. De Charette, E. Wirbel, X. Perrotton, and F. Nashashibi, “Sparse and dense data with cnns: Depth completion and semantic segmentation,” *international conference on 3d vision*, pp. 52–60, 2018.
- [41] D. Wofk, F. Ma, T. Yang, S. Karaman, and V. Sze, “Fastdepth: Fast monocular depth estimation on embedded systems,” *arXiv: Computer Vision and Pattern Recognition*, 2019.
- [42] V. Nekrasov, C. Shen, and I. Reid, “Light-weight refinenet for real-time semantic segmentation,” *arXiv preprint arXiv:1810.03272*, 2018.
- [43] A. Das, S. Kandan, S. Yogamani, and P. Krizek, “Design of real-time semantic segmentation decoder for automated driving,” *arXiv preprint arXiv:1901.06580*, 2019.
- [44] J. Ku, A. Harakeh, and S. L. Waslander, “In defense of classical image processing: Fast depth completion on the cpu,” pp. 16–22, 2018.